Check for updates

Mechanically robust, multifunctional and nanofibrous membranes for tuberculosis elimination†

Nakarin Subjalearndee and Varol Intasanta ID *

M. tuberculosis H37Ra is one of the most virulent microbes in the world; it causes endemic and neglected disease that is highly drug resistant, and no vaccine has yet been created for it. In this present study, mechanically robust and potent antibacterial membranes were fabricated for total elimination of water and airborne tuberculosis (TB) bacteria. *Via* simple electrospinning, a multi-component, water-based solution containing nanofunctional and antibacterial materials led to a thermally and chemically stable nanofibrous membrane with water-repellent, UV-resistant, and antibacterial properties. The liquid- and air-permeable multifunctional nanofibrous membrane contains distributed fibers with two distinct characteristic sizes, proven to be unique physical origins of its exceptional sharp tensile strength and elongation percentage. Concerns over the unfavorable release of nanosilver into the environment and human respiratory systems were palliated by a unique approach for *in situ* formation of a chemical network that trapped the concerned entities. The nanomembrane not only could effectively filter the *M. tuberculosis* H37Ra bacteria, but could also completely exterminate them by a process involving cell membrane destabilization *via* direct contact of the inherently intact lipid–protein bilayers with the nanofibrous network with embedded lethal nanosilver. Finally, the persistent physical integrity of the membrane after harsh simulated weathering indicates its potential and extended usage as a nanofilter in remote areas where TB is endemic.

1. Introduction

Nanofibrous membranes are an important topic in science, technology, and a broad spectrum of product development.[1,2] Disorderly deposition of nanofibers onto a substrate leads to ultrathin and light-weight nonwoven nanofibers with minuscule pores distributed among nanofibrous structures of the membranes. The sizes of the pores are directly influenced by the sizes of the fibers and their spatial alignment. It has been well established that nanofibrous membranes show promise in broad applications such as in nanofiltration,[3,4] separation,[5] catalysis,[6] and biomedical engineering.[7]

However, as small fibers create small pores with apparently superior efficiency for several applications such as filtration, the mechanical strength of the membrane tends to decrease and become problematic in device fabrication. Since the chemical and physical characteristics of nanofibers and nanofibrous membrane directly dictate both their functions and strength,[8]

Nano Functional Textile Laboratory, National Nanotechnology Center, National Science and Technology Development Agency, 111 Phahonyothin Road, Klong Nueng, Klong Luang, Pathumthani, 12120, Thailand. E-mail: varol@nanotec.or.th; Fax: +66-2564-6981; Tel: +66-2564-7100 ext. 6580

to advance this membrane technology and make effective use of nanofibrous membranes, their functions, mechanical strength, and structural integrity become crucial issues.

Tuberculosis (TB) is one of the leading neglected diseases worldwide; it is caused by TB bacteria. The microbes can be transmitted through air *via* miniscule liquid vesicles generated by coughing, sneezing, and speaking.[9] Recently, the recurrence of infection cases in several regions around the globe is a harbinger of a TB pandemic. Drugs with adverse side-effects and multi-drug cocktails are often used because most new TB patients are infected with resistant bacteria.[10–12] Moreover, the research and development of new TB vaccines has not resulted in successful clinical trials.[13,14] For these reasons, a preventive approach towards TB infection becomes one of the most promising approaches to address the impending pandemic.

TB microbes are transmitted through air *via* aerosols containing bacteria mainly generated from infected patients. As only a few bacterial TB cells per cubic meter can cause infection,[15] protection against the disease by entrapment of the airborne bacteria could be considered as an effective preventive approach. As a universal protective measure against several microbial outbreaks, air filtration can be carried out using face masks, portable filters, and ventilation systems.[16,17] Given that the smaller the pores of the filter, the better the filtration efficiency, nanofilters have emerged as one of the most promising

tools to eliminate microbial particles *via* a size-exclusion approach while allowing clean air to flow through.

Although it has been reported that a polycarbonate filter membrane has been used as a part of TB diagnosis by employing a small membrane filtration (SMF) method,[18,19] no previous studies have reported the use of nanofibrous membranes for TB elimination. However, there are reports on the research and development of functional nanofibrous membranes for broad applications. Souzandeh *et al.* have reported polymer/protein composite nanofibrous membranes *via* electrospinning for filtration applications; they have found that the membrane shows excellent filtration efficiency not only for airborne particulates but also for poisonous gases such as formaldehyde and carbon monoxide.[20] In addition, Gopal *et al.* have reported nanofibrous membranes from polysulfone polymers with efficiency for micro-particle removal from wastewater.[21] Moreover, Lala *et al.* have reported antimicrobial nanofibrous membranes fabricated from a variety of polymers containing $AgNO_3$ *via* electrospinning. It has been found that the combination of PAN and 5 wt% $AgNO_3$ leads to the most effective bacterial elimination.[22] It can be seen that no filters have been reported for both blocking and killing TB cells.

It can be seen that research and development on the fabrication of nanofibers and nanofibrous membranes has significantly advanced. While the use of nanofibrous membranes for ultrafine filtration of airborne particles is prevalent, their applications for antibacterial air filtration are limited. Most importantly, the use of nanofibrous membranes for physical barriers of TB bacteria has long been unexplored.

In the present study, we explored multifunctional nanofibrous membranes for the airborne elimination of bacteria. Mechanically robust and potent antibacterial membranes were fabricated for total elimination of water and airborne tuberculosis (TB) bacteria. *Via* simple electrospinning, a deliberately-designed, multi-component, water-based solution with nano-functional and antibacterial materials was fabricated into a thermally and chemically stable nanofibrous membrane with water repellent, UV-resistant, and antibacterial properties. The chemical and physical structures of the nanomembranes were investigated by SEM and IR and correlated with the resulting functional and mechanical properties. Concerns regarding the unfavorable release of nanosilver, the most potent antibacterial agent, into the environment and human physiological and respiratory systems needed to be addressed. The nano-membranes were applied for filtration of water and airborne *M. tuberculosis* H37Ra bacteria. Moreover, the physical integrity of the nanomembrane was tested under harsh simulated weathering to confirm its potential for extended usage in remote and rural areas where TB is endemic.

2. Experimental

2.1 Materials

Mowiol 40-88 (polyvinyl alcohol, PVA, M_w ~205 000 g mol^{-1}), silver nitrate, silver nanopowder, zinc acetate dihydrate, and glutaraldehyde solution (50 wt% in water) were of analytical grade and purchased from Sigma Aldrich, Bangkok, Thailand.

Zinc oxide nanoparticles (Nano Materials Technology Co., Ltd., Chonburi, Thailand) and perfluoroalkyl acrylate copolymer emulsion (Archroma Co., Ltd., Bangkok, Thailand) were of commercial grade. All chemicals were used as received.

2.2 Preparation of electrospinning precursors for multifunctional nanofibrous membranes

The following protocol has been provided as an example. A PVA solution was prepared by adding PVA (2 g) to deionized water (18 g) under magnetic stirring with applied heat at 80 °C for two hours. Subsequently, silver nitrate (0.2 g), zinc acetate (0.2 g), silver nanopowder (0.1 g), zinc oxide nanoparticles (0.1 g), and perfluoroalkyl acrylate copolymer emulsion (4 g) were added to the PVA solution under magnetic stirring for 30 minutes followed by sonication for 30 minutes. Then, glutaraldehyde solution (4 g) was added to the abovementioned solution under magnetic stirring for 5 minutes.[23]

2.3 Fabrication of multifunctional nanofibrous membranes by a Nanospider machine

For pre-pilot scale nanofiber fabrication using a Nanospider machine (NS LAB 500), the precursor solution (30 ml) was transferred into a 50 ml semi-cylindrical chamber. The distance between the rotating wire electrode and the ground electrode was adjusted to 18 cm. During the fabrication process, the ground electrode was rotated at 5 rpm under an applied voltage of 55 kV. After spinning, the resulting nanofibrous membrane was dried in a hot air oven at 140 °C for an hour. As indicated in the Results and discussion section, GA 10 represents nanofibers with PVA and glutaraldehyde, GA 10_A represents nanofibers with PVA, glutaraldehyde, silver nitrate, silver nanoparticles, zinc acetate, and zinc oxide nanoparticles, PF 10_A represents nanofibers with PVA, perfluoroalkyl acrylate copolymer emulsion, silver nitrate, silver nanoparticles, zinc acetate, and zinc oxide nanoparticles, and GA/PF 10_A represents nanofibers with PVA, glutaraldehyde, perfluoroalkyl acrylate copolymer emulsion, silver nitrate, silver nanoparticles, zinc acetate, and zinc oxide nanoparticles.

2.4 Multifunctional nanofibrous membrane characterization by electron microscopy

The morphologies of the nanofibers were characterized using a scanning electron microscope (SEM, S3400N, 20 kV, working distance of 5–7 mm; SEM-EDX, 20 kV, working distance of 10 mm).

2.5 Fourier transform infrared spectroscopy (FTIR)

The chemical characteristics of the multifunctional nanofibrous membranes were characterized by FTIR (Micro ATR, Model: Nicolet 6700 FT-IR, Thermo Scientific, USA).

2.6 Contact angle measurements

Contact angle measurements were performed using a tensiometer (Dataphysics Instruments, TC/TPC 150) to quantify the water repellency levels of the nanofibers. First, an electrospun

membrane was placed on a sample stage. Then, a 1 μl water droplet was dispensed on the surface prior to contact angle measurement. An averaged value has been reported from five measurements on different areas.

2.7 Multifunctional nanofibrous membrane characterization by tensile strength measurements

The tensile strengths of the nanofibrous membranes were determined using a tensile testing machine (Instron model 5566). The nanofibrous membranes were cut into 1 inch × 2 inch pieces at a 100 mm min^{-1} extension rate with a gauge length of 20 mm[8]. Following the ASTM G 154:2006 method, the simulated weathering conditions consisted of UVA irradiation (340 nm, 0.8 W m^{-2}) at 60 ± 3 °C for 8 hours before moisture condensation at 50 ± 3 °C for 4 hours.

2.8 Ultraviolet protection factor (UPF) and transmittance percentage testing

Both the ultraviolet protection factors (UPF) and UV transmittance percentages of the nanofibers were quantified by the AATCC 183:2010 method.

2.9 Antibacterial activity testing

Antibacterial testing was performed against representative Gram positive and Gram negative bacteria, *i.e. Staphylococcus aureus* and *Klebsiella pneumoniae*, respectively. The anti-*M. tuberculosis* H37Ra properties were evaluated by water and air filtration.

2.9.1 *Staphylococcus aureus* and *Klebsiella pneumoniae*. The primary antibacterial testing activities were performed using the AATCC TM 100:2004 and AATCC TM 147:2011 standard testing methods. For both testing standards, *Staphylococcus aureus* and *Klebsiella pneumoniae* were selected as Gram positive and negative model bacteria, respectively.

2.9.2 *M. tuberculosis* H37Ra. The *M. tuberculosis* H37Ra elimination efficiency was evaluated through water filtration in a class II biosafety cabinet; the aerosol filtration was evaluated in a class III biosafety cabinet.

2.10 Preparation of mycobacterial cell suspensions

The *M. tuberculosis* H37Ra cell suspension was prepared in a class II biosafety cabinet. First, three to four loops-full of a logarithmic phase mycobacterial culture were suspended in a tube containing 5–6 glass beads. Subsequently, the mycobacterial cells were beaten with Middlebrook 7H9 broth supplemented with 10% OADC until the mycobacterial clumps were dispersed completely; the large clumps were then allowed to settle for 20 min at room temperature. Last, 100 μl cell suspension was inoculated into Middlebrook 7H9 broth supplemented with 10% OADC incubate at 37 °C with interval shaking to reach a McFarland turbidity of 1 (1–3 × 10^7 cfu ml^{-1}).[24]

2.11 *M. tuberculosis* H37Ra elimination efficiency testing by water media filtration in a class II biosafety cabinet

First, the nanofibrous membranes were cut into square shapes with diameters of 2.5 cm. Subsequently, the cut membrane was inserted into a filter holder (Sartorius, Göttingen, Germany) and autoclaved for 15 minutes at 121 °C 15 lb in^{-2} before being dried overnight at 60 °C for sterilization. In the filtration step, one ml of each diluted suspension was aliquoted by a commercial syringe (TERUMO®SYRINGE, Tokyo, Japan) and then filtered through a sterilized nanofibrous membrane or a Sartorius membrane (pore size 0.45 μm) used as a reference by pushing with the thumb. After filtration, 100 μl of filtrate solution was placed on Middlebrook 7H10 agar followed by incubation at 37 °C for 3–4 weeks. Prior to incubation at 37 °C for 2–10 days, the membrane was cautiously opened in a sterile Petri dish and cut into small pieces of approximately 1–5 mm × 4–10 mm. Later, a piece of the membrane was transferred to a well of a 96-well microtiter plate or glass slide. A Live/Dead staining kit (1IVM-L7012 LIVE/DEAD BACLIGHT, Invitrogen, USA) was utilized to determine the mortality of the cells.[25] For image processing detection, a confocal laser scanning microscope (Nikon, ECLIPSE Ti, Japan) was employed.

2.12 *M. tuberculosis* H37Ra elimination efficiency testing by aerosol spray filtration in a class III biosafety cabinet

To start, *M. tuberculosis* H37Ra was grown on the Lowenstein–Jensen (LJ) medium at 37 °C for 3–4 weeks prior to preparation of the cell suspension. Subsequently, a single cell suspension was prepared in 0.85% NaCl to obtain a turbidity of 1 McFarland. The cell suspension was ten-fold diluted from 1–3 × 10^6 to 10^7 for further usage. Each one milliliter of *M. tuberculosis* H37Ra with 1–3 × 10^6 cell concentration was filled in a sterilized atomizer syringe (LMA MAD NasalTM, Teleflex, USA) one milliliter into the readily pleated cartridge nanofibrous membrane through a plastic funnel fixed on the cartridge. All the processes were performed in the class III biosafety cabinet in the biosafety III laboratory at the Faculty of Veterinary Science, Mahidol University, Thailand. After filtration, different areas on the cartridge under the projected scope of the funnel were selected, and a small piece was cut and transferred onto the surface of an M7H10 or water agar plate. Each piece was marked on its front and back sides, on which the number of mycobacteria was determined before incubation; the pieces were then stained using a Live/Dead staining kit for 6 days. During incubation, 3 sampling areas of the sprayed nanofibrous membrane were cut and viewed using a confocal microscope after 24, 48, 72, 96, and 168 hours to qualitatively determine the numbers of live and dead mycobacterial cells on the membranes according to eqn (1).[26]

$$\text{Elimination percentage (\%)} = \text{dead TB cells}/\text{total TB cells} \times 100 \quad (1)$$

3. Results and discussion

While functional nanofibers can be simply derived from functional spinning precursors, the fabrication of multifunctional nanofibrous membranes faces several technical challenges including compatibility among the components and stability of the precursor solution as well as the manifestation of these competing functional components. The key concepts for the practical utilization of nanofibrous membranes involve the development of both functional and mechanical strength.[27]

In this study, mechanically robust, flexible, and multifunctional nanofibrous membranes with potent antibacterial functions were fabricated from a charge-stabilized multicomponent nanocolloid *via* facile and scalable needle-free Nanospider electrospinning. With unique functions, the nanomembranes contain a unique combination of commercially available and cost-effective functional materials. The spinning process was made possible by the presence of water-soluble polyvinyl alcohol (PVA) among well-dispersed and nanosized additives.[28–30] Dangling hydroxyl groups were specifically chosen to act as a molecular platform for further chemical crosslinking during the post-spinning heat-assisted mechanical development process.

At first, functional materials providing water repellence, anti-UV properties, mechanical stabilization, and antibacterial function were deliberately included during the material design process. The water-repellent function was expected to contribute to self-cleaning and non-stick features *via* low surface energy. The anti-UV material was used for molecular stabilization against environmental light while maintaining the chemical and physical stability of the nanomembrane.[31,32] In addition, a crosslinking agent was employed to form a molecular network within nanofibers and stable physical crosslinking between nonwoven nanofibers.

While multiple auxiliary functions can help improve ease of usage and nanomembrane stability, the central functional development idea focused on the development of antibacterial properties. The most important antibacterial additive for this design is silver nanoparticles, which have been shown to have the most potent antibacterial properties against a broad range of bacterial strains.[33] The silver nanoparticles were responsible for killing micron-sized TB cells *via* contact mode when the bacteria were trapped on nanopores within nanofibrous membranes.

3.1   Nanofibrous membrane fabrication and characterization

3.1.1   Multifunctional nanofibrous membrane fabrication.
The crosslinkable hydroxyl side groups on polyvinyl alcohol (PVA) offered a simple route for the formation of a permanent chemical bonding network.[34] First, a precursor solution containing both the polymer and glutaraldehyde (GA) was prepared, and its compatibility and stability were studied as a function of the solid content and mass ratio between the two entities. Experimentally, three variations of the PVA to GA ratio, *i.e.* 1 : 0.5, 1 : 1, and 1 : 2 (weight to weight ratio), were prepared with 10 wt% PVA solution before the electrospinning process *via*

Nanospider. At a 1 : 0.5 ratio, bead-free, homogeneous nonwoven nanofibers were observed by SEM (Fig. S1a, ESI†). Post-spinning heat treatment at 140 °C for an hour was performed to activate the formation of a chemical bonding network of both GA and PVA. No distinct physical transformation among the nanofibers was apparent after curing (Fig. S1b, ESI†). To primarily evaluate the structural stability of the nanomembrane, a 1 cm × 1 cm piece of nanomembrane was immersed in water for 5 minutes and dried at room temperature (Fig. S2a, ESI†). The SEM analysis of the latter showed that the nanofibrous membrane had collapsed into a thin film with no trace of fibrous structures (Fig. S1c, ESI†). It could be deduced from the drastic structural transformation that the crosslinking was not effective.

Next, the percentage of GA was increased to achieve a weight ratio of PVA to GA of 1 : 1 in the hope that the crosslinking would be more effective (Fig. S1d, ESI†). Similarly to the 1 : 0.5 ratio in the previous example, post-spinning heating had no effect on the physical character of the nanofibers (Fig. S1e, ESI†). However, their physical structure was slightly perturbed during stability evaluation under water as the fibers appeared to merge with those in the vicinity (Fig. S1f, ESI†). Although physical integrity could not be achieved at this step, it could be confirmed by the result that GA played a key role in stability improvement of the nanomembrane.

At a 1 : 2 ratio of PVA to GA, spinning resulted in a well-defined nanofibrous membrane (Fig. 1a) as post-spinning curing did not change the structure (Fig. S2a, ESI†). Under prolonged immersion in water, the nanomembrane showed a certain degree of physical integrity, with some slightly merged nanofibers in the cross-over area (Fig. 1b). Although increasing
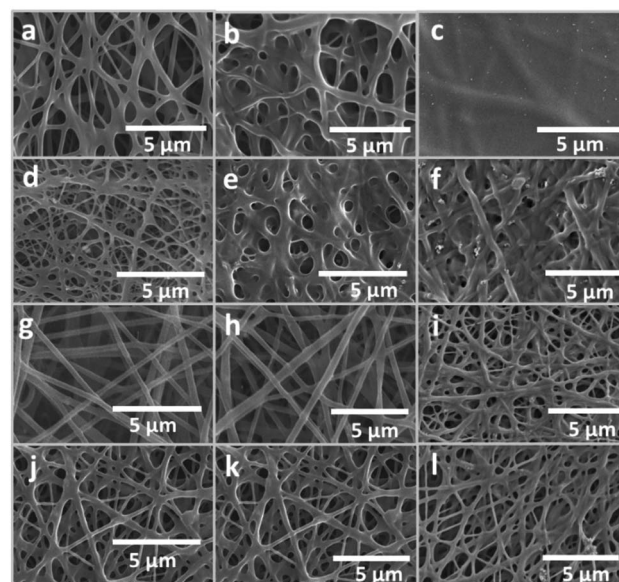

Fig. 1 SEM images of the (a) GA 10, (d) GA 10_A, (g) PF 10_A, and (j) GA/PF 10_A nanofibers. SEM images of the (b) GA 10, (e) GA 10_A, (h) PF 10_A, and (k) GA/PF 10_A nanofibers after immersion in water. SEM images of (c) GA 10, (f) GA 10_A, (i) PF 10_A, and (l) GA/PF 10_A nanofibers after exposure to simulated weathering conditions.

the GA percentage in the PVA solution led to nanofibers with improved water resistance, the respective electrospinning process suffered from a drastic increase in viscosity and the glue-like solution that produced inhomogeneous nanofibers and ill-defined nanofibrous membranes. As a result, a 1 : 2 weight ratio of PVA to GA was concluded to be the optimized condition for producing a water-resistant PVA nanofibrous membrane.

Furthermore, the anti-weathering properties of the water-resistant nanofibrous membrane have been studied using the ASTM G 154:2006 standard for textiles that employs UV exposure and condensation processes. Experimentally, the membrane was irradiated under UV-A (340 nm) at 60 °C for 8 hours before condensation at 50 °C for 4 hours. The protocol represents actual conditions of the prolonged exposure to an outdoor environment, where the presence of moisture and UV irradiation may be dominant. As a result, the micropores within the nanofibrous membrane entirely collapsed into a thin, flat film (Fig. 1c). This implied that the combination of the crosslinker and polymer was insufficient to create a nanofibrous membrane with anti-weathering properties.

After improving the moisture- and UV-resistant properties of the nanomembranes, a new generation of nanomembranes was designed to include stability-enhancer additives. With a broad range of future applications, such as in filtration and microbial elimination, anti-UV and antibacterial additives were introduced into the electrospinning pre-cursor solution. After the addition of silver nitrate, zinc acetate, silver nanopowder, and zinc oxide nanoparticles to the polymer solution in a fixed order, the resulting precursor solution appeared dark gray in color. After nanofiber fabrication *via* the Nanospider machine, SEM analysis revealed nanofibers with a higher degree of crosslinking in comparison with the GA_10 nanofibers (Fig. 1d). After heat treatment, the physical character of the membrane remained intact (Fig. S2b, ESI†); this indicated the thermal stability of the polymer in the presence of functional additives. To confirm the presence of silver and zinc nanoparticles, SEM-EDX analysis was performed to detect and qualitatively enumerate the silver and zinc contents within nanofibers (Fig. S3, ESI†). Consequently, the prominent appearance of the two elements proved the success of the fabrication process. Moreover, the water resistance of the additive-containing nanomembrane was evaluated by dipping the sample into water. The nanofibrous membrane manifested swelling (Fig. 1e). After exposure to simulated weathering, the nanomembrane remained mostly intact; however, it showed a more serious degree of swelling in comparison with that observed in the abovementioned water immersion experiment (Fig. 1f). It can be inferred from this finding that addition of anti-UV and antibacterial additives to the water-resistant nanofibers helped to improve their physical stability against moisture and UV exposure. However, undesirable merging and swelling of the constituting nanofibers following weathering exposure resulted in a partially-collapsed porous structure that might affect filtration efficiency in future applications.

The observation of swelling for previous nanofibrous prototypes suggests the relevance of the solubility parameter and the surface energy of PVA. As swelling is a phenomenon in which two materials of comparable solubility parameters dissolve together, penetration of water into the crosslinked PVA suggests that these values for these two chemicals are similar to a certain degree. Furthermore, the undesirable PVA–water interface may also be due to the high surface energies of both crosslinked and non-crosslinked PVA. Therefore, it was hypothesized that modification of the chemical composition of the matrix of the nanofibers could change both its solubility parameter and surface tension. While the solubility parameter could be changed *via* both decreasing and increasing the value, the surface energy could only be lowered to prevent the formation of the PVA–water interface.

In the next experiment, this hypothesis was tested by replacing GA with perfluoroalkyl acrylate copolymer emulsion (PF). This replacement not only would result in lower surface energy mainly due to the inherent characteristics of the copolymer, but would also enable a change in the viscosity in the absence of chemical bonding caused by GA. With this molecular-level setup, any improvement in physical stability must be due to changes in viscosity and surface energy; this verifies the established hypothesis. As a result, SEM analysis of the as-spun sample showed no undesirable merging between the nanofibers; this is vastly different from the previous observations for the GA 10 and GA 10_A nanofibers (Fig. 1g). The nanostructure also remained perfectly intact after heat treatment (Fig. S2c, ESI†). In addition, the presence of fluorine element was confirmed by the SEM-EDX technique (Fig. S3c, ESI†). Apparently, the GA-free nanofibrous membrane revealed excellent water-resistant functions in comparison with the previous prototypes made with GA (Fig. 1h). Furthermore, under simulated weathering conditions, the GA-free and water-resistant nanomembrane developed into a slightly swollen fibrous structure, as compared to the GA 10_A nanofibrous membrane (Fig. 1i). The enhanced stability implied the positive effects of the changes in the solubility parameter and surface energy upon replacement of GA with the perfluoroalkyl acrylate copolymer.

The abovementioned results indicated two relevant aspects of stability in this study—physical stability *via* GA crosslinking formation and chemical stability *via* the effects of the perfluoro compound on the surface energy. Following this rationale, the combination of two additives, *i.e.* GA and PF, was realized in subsequent fabrication. For the as-spun sample, SEM analysis showed a moderate crosslinking degree as compared to that of previous samples made with either GA or PF (Fig. 1j). The GA/PF-containing membrane maintained its well-defined nanofibrous structure after heat treatment (Fig. S2d, ESI†) and prolonged immersion in water (Fig. 1k). Furthermore, the nanomembrane showed a minimal degree of swelling upon exposure to weathering conditions in comparison with the previous membrane prepared without GA and PF (Fig. 1l). It can be concluded that both the chemical crosslinkers, such as GA, and surface energy modifiers, such as PF, can function synergistically to improve moisture and UV resistance in PVA.

3.2 Structural analysis and unique crosslinking morphology

From primary characterization of the crosslinked nanofibers by SEM, it was found that different types of crosslinking structures were formed within the bulk of the nanofibrous membranes. Interestingly, three different types of crosslinking were observed for the GA 10_A, PF 10_A, and GA/PF 10_A nanofibers. Fig. 2a illustrates the characteristic crosslinking of GA 10_A, which shows tight merging of fibers with large diameters (Fig. 2a). However, homogeneity and a low merging degree were observed in the PF 10_A nanofibrous membrane (Fig. 2b). Finally, the GA/PF 10_A nanomembrane possessed more distinctive characteristics of crosslinked nanofibers (Fig. 2c). Evidently, nanofibers with two different diameters, seemingly inherited from those representative of GA 10_A and PF 10_A, appeared simultaneously in GA/PF 10_A. It can be hypothesized that the chemical interactions between GA or PF molecules and PVA had independent effects.

Surface wetting analysis was conducted, where the contact angles for GA 10_A, PF 10_A, and GA/PF 10_A nanomembranes were measured using a tensiometer. GA 10_A showed the lowest contact angle at 96.17°. This result confirmed the low hydrophobicity of the sample; this partially explained low stability during the anti-weathering effect test. The increased contact angles for both the PF 10_A and GA/PF 10_A nanomembranes at 136° and 135.40°, respectively, can be attributed to the presence of PF molecules on the surface of the nanofibers.

3.3 Fourier transform infrared spectroscopy (FTIR) characterization

The chemical characteristics and molecular bonding between the hydroxyl groups of PVA and the aldehyde groups of GA were

confirmed by FTIR. In addition, hydrogen bonding between PVA and PF was revealed by the chemical shift at the O–H stretching position. Herein, four major absorption bands, as shown in Fig. 3, represent the O–H, C–H, C=O, and C–F stretching vibrations. The largest band in the range 3200–3600 cm^{-1} indicated the O–H stretching vibrations of the hydroxyl groups under both intermolecular and intramolecular bonding. The O–H stretching peak intensity of the non-crosslinked PVA molecules was higher than that of the crosslinked/reacted PVA molecules due to the reduced degrees of freedom of the hydroxyl groups after the chemical reaction among available hydroxyl groups on PVA and GA as well as hydrogen bond formation with PF molecules.[35] In addition, the chemical shift, as shown in Fig. 3 (positions i and iv), signified the strength of intermolecular hydrogen bonding between hydroxyl groups on PVA.[36] The peak of maximum intensity of the PVA nanofibers at the position i (3289 cm^{-1}) was shifted to 3322 cm^{-1} in PF 10_A, as indicated by position iv. This observation implies that weak intermolecular interactions between PVA molecules occurred possibly because of interruptions due to the formation of H–F bonds by the PF molecules. In contrast, the maximum absorption peak of the GA 10 sample was shifted from 3289 cm^{-1} to 3267 cm^{-1}. This latter observation indicated that strong intermolecular hydrogen bonding occurred between PVA molecules possibly because the GA crosslinker limited the spatial movement of the PVA molecules. As such, the hydroxyl groups can form stronger intermolecular hydrogen bonds.

3.4 Tensile strength testing

The mechanical and dimensional integrities of the nanofibrous membranes with controlled thickness were evaluated via tensile strength and elongation percentage. To observe the stability after recycling, the nanofibers after exposure to weathering effects were also examined for comparison with the as-spun nanofibers (Table S1, ESI†). The tensile strength results of the GA 10 nanofibers before and after exposure to weathering effects were drastically different (Fig. 4a). The tensile strength of the as-spun nanofibers was averaged to be 5.27 N, and their
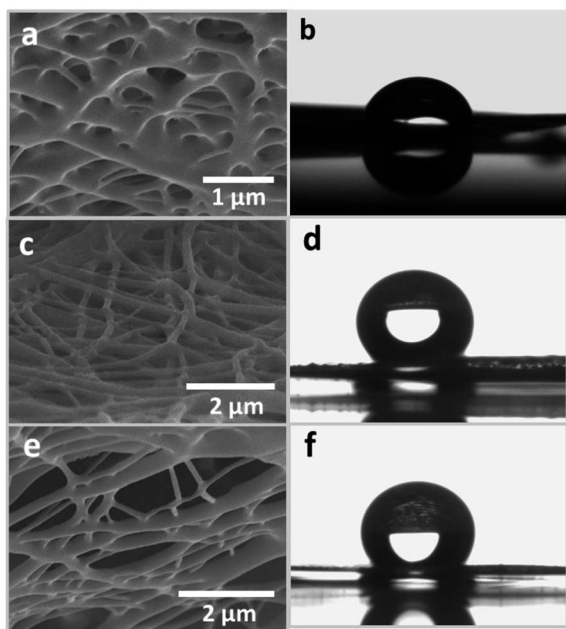

Fig. 2 The crosslinking character of the (a) GA 10_A, (c) PF 10_A and (e) GA/PF 10_A nanofibers. Contact angles of the (b) GA 10_A, (d) PF 10_A and (f) GA/PF 10_A nanomembranes.
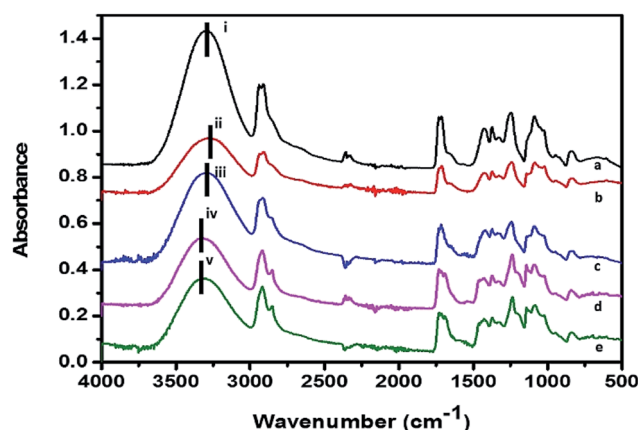

Fig. 3 FTIR spectra of the (a) PVA, (b) GA 10, (c) GA 10_A, (d) PF 10_A, and (e) GA/PF 10_A nanomembranes.
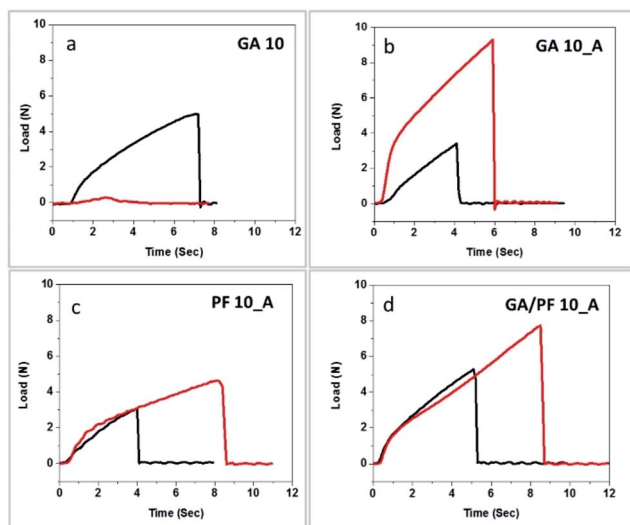
Fig. 4 Tensile strength profiles of the (a) GA 10, (b) GA 10_A, (c) PF 10_A, and (d) GA/PF 10_A nanomembranes before (black line) and after (red line) exposure to simulated weathering conditions.

elongation was 54.45%. After exposure to the weathering effects, both parameters decreased to 0.44 N and 21.67%. The dramatic decreases in both parameters after exposure to weathering effects is consistent with the transformation of the nanofibers into a thin film previously revealed by SEM. Contrasting phenomena were observed for the GA 10_A membrane. After exposure of the membrane to weathering effects, the tensile strength and elongation percentage increased from 2.98 N and 31.11% to 10.67 N and 35.00%, respectively (Fig. 4b). These results were also consistent with the previous SEM observations in terms of the swelling and merging of nanofibers after this treatment. Although the seemingly crosslinked nanofibers offered higher tensile strength, their reduced porosity as a consequence of collapsed internal pores was inevitable.

As illustrated in Fig. 4c, the tensile strength and elongation of the PF 10_A membrane increased by 43.1% and 36.67%, respectively, after exposure to weathering effects. Apparently, the elongation percentage of the treated samples was almost 12 times higher than that of treated GA 10_A membrane. It can be said that the PF 10_A membrane possessed higher flexibility after exposure to weathering effects than the GA 10_A membrane. It was hypothesized that perfluorocarbon might have played a role in both the composition and molecular structure of the membrane, which helped improve its resistance to weathering effects.

Fig. 4d presents the interesting mechanical characteristics of GA/PF 10_A. Incidentally, the combination of glutaraldehyde and perfluorocarbon resulted in the highest tensile strength and elongation percentage after exposure to weathering effects (Fig. 4d). The tensile strength and elongation percentage were increased from 4.08 N and 35.56% to 6.68 N and 73%, respectively. Evidently, the simulated weathering conditions transformed the nanofibrous membrane into a crosslinked film. It was hypothesized that the resulting crosslinked polymers inherited better mechanical strength than their nanofibrous

counterparts and showed improved tensile strength and elongation percentage after exposure. In addition, the collapse profile of GA/PF 10 was additionally scrutinized to understand the physical transformation mechanism and the origin of the mechanical strength of GA/PF 10. The fracture mechanics profile can be divided into 4 regions: the threshold (non-stretching nanofibers) period, the elongation (stretched nanofibers) period, the overstretching (breaking of intermolecular crosslinking) period and, finally the failure (nanofiber structure collapsing) period (Fig. 5a). Fig. 5b shows the first period, where the nanofibers are aligned randomly. Subsequently, the nanofibers were somewhat aligned and stretched, as clearly observed by SEM (Fig. 5c), in the second stage. The third and longest period in the tensile strength profile (Fig. 5a, point iii) represented the breaking of the intermolecular crosslinking (Fig. 5d), where the nanofibers were significantly and directionally aligned. Finally, the last period (Fig. 5a, point iv) showed collapsing of the nanofiber structures (Fig. 5e).

3.5 Multifunctional property evaluation: ultraviolet (UV) protection and transmittance

The anti-UV properties of the nanofibrous membranes were measured according to the AATCC 183:2010 standard testing method. The membrane conditions were divided into dry and wet under the three tested parameters: ultraviolet protection factor (UPF), UV-A transmittance percentage, and UV-B transmittance percentage (Table S2, ESI†). The UPF values of the PF 10_A and GA/PF 10_A membranes showed the highest values of 50+ under both wet and dry conditions. Similarly, the GA 10_A membrane showed 50+ UPF under dry conditions and 32 under wet conditions. Last, the GA_10 membrane possessed the lowest UPF values under both the wet and dry conditions (7 and 3, respectively).

The UV-A and UV-B transmittances of the PF 10_A membrane were slightly higher than those of the GA/PF 10_A membrane (less 0.1% difference) under both membrane conditions. For the GA 10_A membrane, the two transmittance values under dry conditions were 0.2%, whereas under wet conditions, the UV-B transmittance was higher than the UV-A transmittance by 0.5%. Based on these results, the membrane with the highest UV transmittance percentage was GA 10. For this membrane, the value under the wet conditions was
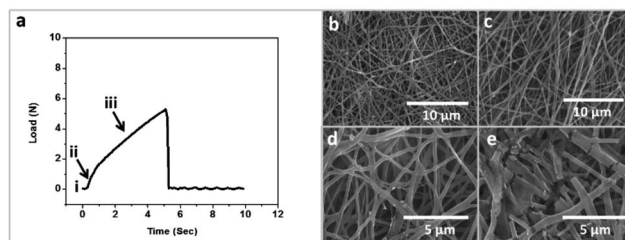

Fig. 5 (a) Nanofiber structure collapsing profile of GA/PF 10_A showing (b) non-stretching nanofibers, (c) stretched nanofibers, (d) breaking of intermolecular crosslinking, and (e) the collapsed nanofiber structure.

approximately two times higher than that under the dry conditions.

3.6 Primary antibacterial properties

The primary anti-bacterial properties of the nanofibrous membranes were measured according to the AATCC TM 100:2004 and AATCC TM 147:2011 standard testing methods (Table S3, ESI†). The first standard evaluates the anti-bacterial properties by dynamic contact in liquid media within 24 hours, whereas the second standard measures the zone of bacteria inhibition on agar plates. Under the AATCC TM 100:2004 standard, all nanofibrous membranes showed more than 99.9% efficiency towards elimination of representative Gram positive and negative bacteria. In the AATCC TM 147:2011 test, the GA_10 membrane showed no anti-bacterial properties, whereas the rest of the membranes showed clear anti-bacterial properties with varying zones of inhibition. Evidently, the GA/PF 10_A membrane possessed the largest inhibition zone (Fig. S5, ESI†).

3.7 Anti-tuberculosis properties for water-borne TB

M. smegmatis mc^{2}155 was selected as a representative in the anti-tuberculosis water filtration experiment. A commercially

Fig. 6 Confocal laser scanning microscopy images showing dead (red) and living (green) M. smegmatis mc^{2}155 cells on (a–c) Satorius cellulose membrane (pore size of 0.45 μm), (d–f) GA 10, (g–i) GA 10_A, (j–l) PF 10_A, and (m–o) GA/PF 10_A nanomembranes after liquid filtration.

available cellulose membrane with a pore size of 0.45 microns (Sartorius membrane) was used as a reference. Fig. 6 shows dead (red), living (green), and merged-image (green and red) cells of M. smegmatis mc^{2}155 on the membranes after filtration. The filtrate obtained from the Sartorius membrane contained living bacteria (green dots) with no observable dead bacteria (red dots) on the membrane (Fig. 6a–c). Similarly, large clusters of green dots were observed on the GA 10 membrane with respect to those of the dead cells (Fig. 6d–f), suggesting the absence of an anti-tuberculosis effect. For the GA_10 membrane, both dead and living cells of M. smegmatis mc^{2}155 were observed (Fig. 6g–i). Finally, PF 10_A and GA/PF 10_A showed the highest anti-TB properties, as seen from the very low numbers of living M. smegmatis mc^{2}155 cells observed on the membranes (Fig. 6j–o). The GA/PF 10_A membrane was selected for further experiments on pre-pilot TB aerosol filtration due to its excellent antibacterial and weathering effect functions. It was noted that after water filtration, all the nanomembranes remained physically intact, as demonstrated by SEM (Fig. S6, ESI†).

3.8 Observation of anti-tuberculosis properties by aerosol filtration

Pre-pilot scale of M. tuberculosis aerosol filtration testing was performed in a class III safety cabinet. The filtration system contained a machine-pleated and framed nanofibrous membrane under operation by an air purifier machine (Fig. 7).

The size of the pleated membrane was designed to fit with a model commercial air purifier machine (Fig. S7, ESI†). The GA/PF 10_A membrane was selected for this study, and the GA 10 membrane was used as a control. After filtration, 3 pieces of the contaminated membrane were incubated for 24, 48, 72, 96, and 168 hours, followed by colony counting for TB elimination percentage calculation according to eqn (1). After 24 hours of incubation, the GA 10 membrane showed 2.94% dead TB (two dead cells from 68 total TB cells). After 48 hours of incubation, the membranes showed no TB elimination properties (zero dead TB cells from 109 total TB cells). Subsequently, a very low TB elimination percentage resulted after 72 hours of incubation (2.04%) with 11 dead TB cells from 538 total TB cells on the
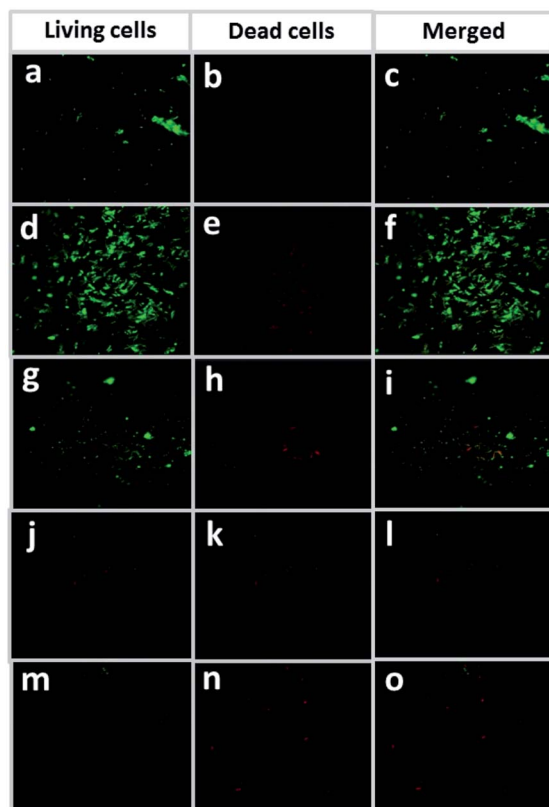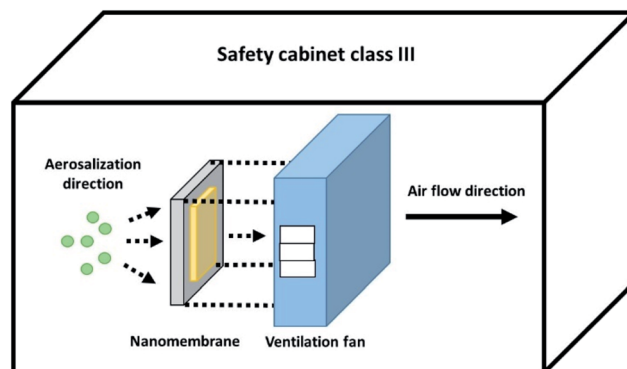

Fig. 7 M. tuberculosis H37Ra aerosol droplet filtration setup scheme inside the class III biosafety cabinet.
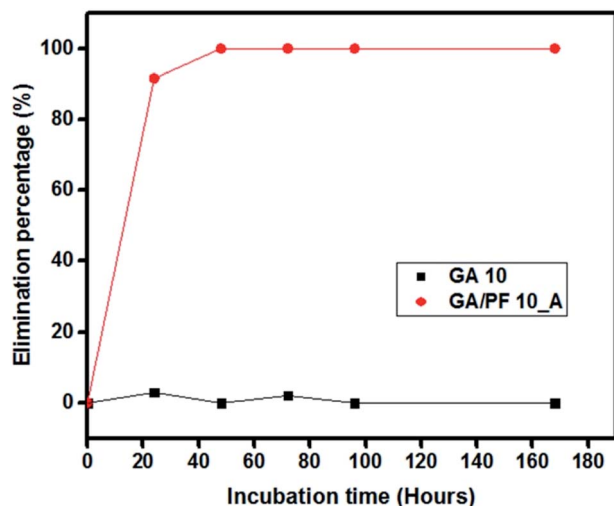
Fig. 8 Cumulative *M. tuberculosis* H37Ra elimination percentage for GA 10 (black) and GA/PF 10_A (red) nanofibrous filters.

membranes. After 96 and 168 hours of incubation, 0% TB elimination was observed on the membranes, with 0 dead TB cells from 104 total TB cells and 0 dead TB cells from 379 total TB cells at 96 and 168 hours of incubation, respectively (Fig. S8, ESI†).

On the other hand, the GA/PF 10_A membrane showed 100% TB elimination after 48 hours of incubation. After 24 hours of incubation, 131 dead TB cells were found on the membranes of 143 total TB cells, which showed 91.61% TB elimination. Moreover, the back side showed no cells of TB trapped on the membrane. At 48, 72, 96, and 168 hours of incubation, all TB cells were dead. Moreover, seventy-four TB cells were found dead on the membrane after 48 hours of incubation, whereas 99, 62, and 70 TB cells were found dead after 72, 96, and 168 hours of incubation, respectively (Fig. S9, ESI†). In addition, the TB cell elimination percentage of GA/PF 10_A was plotted in comparison with that of the control GA 10 membrane (Fig. 8). In conclusion, the GA/PF 10_A membrane showed an exceptional TB killing efficiency of 100% after 48 hours of incubation.

4. Conclusions

Mechanically robust and multifunctional nanomembranes for water and airborne *M. tuberculosis* H37Ra bacteria filtration were successfully fabricated from a charge-stabilized water-based multicomponent nanocolloid *via* Nanospider technology. It was found that the addition of a crosslinking agent helped improve the physical integrity of the nanomembrane. However, the nanomembrane containing a specific combination of crosslinker and perfluoro (PF) compounds showed excellent mechanical strength and flexibility; this was attributed to its unique bimodal-diameter crosslinking characteristics and the hypothetical interruption of PF molecules by the formation of H–F bonds. Moreover, the nanomembrane possessed the highest anti-TB properties in the water phase. For aerosol filtration, 100% of the trapped TB cells on the nanomembrane

were eliminated after 96 hours of incubation. It can be concluded that this nanomembrane has promising qualities for application in remote and rural areas to prevent the spread of TB.

Conflicts of interest

There are no conflicts to declare.

Acknowledgements

References

1 N. Bhardwaj and S. C. Kundu, *Biotechnol. Adv.*, 2010, **28**, 325–347.

2 S. Ramakrishna, K. Fujihara, W. E. Teo, T. Yong, Z. W. Ma and R. Ramaseshan, *Mater. Today*, 2006, **9**, 40–50.

3 F. E. Ahmed, B. S. Lalia and R. Hashaikeh, *Desalination*, 2015, **356**, 15–30.

4 R. S. Barhate and S. Ramakrishna, *J. Membr. Sci.*, 2007, **296**, 1–8.

5 W. J. Ma, Q. L. Zhang, D. W. Hua, R. H. Xiong, J. T. Zhao, W. D. Rao, S. L. Huang, X. X. Zhan, F. Chen and C. B. Huang, *RSC Adv.*, 2016, **6**, 12868–12884.

6 X. W. Mao, G. C. Rutledge and T. A. Hatton, *Nano Today*, 2014, **9**, 405–432.

7 D. Liang, B. S. Hsiao and B. Chu, *Adv. Drug Delivery Rev.*, 2007, **59**, 1392–1412.

8 E. P. S. Tan and C. T. Lim, *Compos. Sci. Technol.*, 2006, **66**, 1102–1111.

9 C. Dye and B. G. Williams, *Science*, 2010, **328**, 856–861.

10 F. Marra, C. A. Marra, N. Bruchet, K. Richardson, S. Moadebi, R. K. Elwood and J. M. FitzGerald, *Int. J. Tubercul. Lung Dis.*, 2007, **11**, 868–875.

11 S. A. Munro, S. A. Lewin, H. J. Smith, M. E. Engel, A. Fretheim and J. Volmink, *PLoS Med.*, 2007, **4**, 1230–1245.

12 R. V. Patel, S. Riyaz and S. W. Park, *Curr. Top. Med. Chem.*, 2014, **14**, 1866–1874.

13 Y. S. Kwon, B. H. Jeong and W. J. Koh, *Curr. Opin. Pulm. Med.*, 2014, **20**, 280–286.

14 Y. S. Kwon and W. J. Koh, *Expert Opin. Invest. Drugs*, 2016, **25**, 183–193.

15 R. Wood, C. Morrow, C. E. Barry, W. A. Bryden, C. J. Call, A. J. Hickey, C. E. Rodes, T. J. Scriba, J. Blackburn, C. Issarow, N. Mulder, J. Woodward, A. Moosa, V. Singh, V. Mizrahi and D. F. Warner, *PLoS One*, 2016, **11**, 1–16.

16 A. S. Dharmadhikari, M. Mphahlele, A. Stoltz, K. Venter, R. Mathebula, T. Masotla, W. Lubbe, M. Pagano, M. First, P. A. Jensen, M. van der Walt and E. A. Nardell, *Am. J. Respir. Crit. Care Med.*, 2012, **185**, 1104–1109.

17 M. M. Zhu, J. Q. Han, F. Wang, W. Shao, R. H. Xiong, Q. L. Zhang, H. Pan, Y. Yang, S. K. Samal, F. Zhang and C. B. Huang, *Macromol. Mater. Eng.*, 2017, **302**, 27.

18 K. P. Fennelly, C. G. Morais, D. J. Hadad, S. Vinhas, R. Dietze and M. Palaci, *J. Clin. Microbiol.*, 2012, **50**, 2096–2099.

19 P. Quinco, S. Buhrer-Sekula, W. Brandao, R. Monte, S. L. Souza, V. Saraceni, M. Palaci, R. Dietze and M. Cordeiro-Santos, *J. Clin. Microbiol.*, 2013, **51**, 2921–2925.

20 H. Souzandeh, K. S. Johnson, Y. Wang, K. Bhamidipaty and W. H. Zhong, *ACS Appl. Mater. Interfaces*, 2016, **8**, 20023–20031.

21 R. Gopal, S. Kaur, C. Y. Feng, C. Chan, S. Ramakrishna, S. Tabe and T. Matsuura, *J. Membr. Sci.*, 2007, **289**, 210–219.

22 N. L. Lala, R. Ramaseshan, B. J. Li, S. Sundarrajan, R. S. Barhate, Y. J. Liu and S. Ramakrishna, *Biotechnol. Bioeng.*, 2007, **97**, 1357–1365.

23 C. Tang, C. Saquing, J. Harding and S. Khan, In Situ Cross-Linking of Electrospun Poly(vinyl alcohol) Nanofibers, *Macromolecules*, 2010, 630–637.

24 N. Cheng, M. A. Porter, L. W. Frick, Y. Nguyen, J. D. Hayden, E. F. Young, M. S. Braunstein, E. A. Hull-Ryde and W. P. Janzen, *PLoS One*, 2014, **9**, e96348.

25 C. M. Davies, *Lett. Appl. Microbiol.*, 1991, **13**, 58–61.

26 P.-S. Chen and C.-S. Li, *Aerosol Sci. Technol.*, 2005, **39**, 371–376.

27 M. H. Al-Saleh and U. Sundararaj, *Composites, Part A*, 2011, **42**, 2126–2142.

28 A. M. M. Sousa, H. K. S. Souza, J. Uknalis, S. C. Liu, M. P. Goncalves and L. S. Liu, *Carbohydr. Polym.*, 2015, **115**, 348–355.

29 Z. W. Li, C. W. Li, Q. Wang, S. J. Shi, M. Hu, Q. Zhang, H. H. Cui, J. B. Sun, M. Zhou, G. L. Wu, J. Z. Dang and L. C. Lu, *J. Biomed. Nanotechnol.*, 2017, **13**, 17–34.

30 C. G. Yuan, S. W. Guo, J. Song, C. Huo, Y. K. Li, B. Gui and X. M. Zhang, *RSC Adv.*, 2017, **7**, 4830–4839.

31 Y. F. Qian, M. J. Qi, L. J. Zheng, M. W. King, L. H. Lv and F. Ye, *Materials*, 2016, **9**, 8.

32 I. Fajzulin, X. M. Zhu and M. Moller, *J. Coat. Technol. Res.*, 2015, **12**, 617–632.

33 J. R. Morones, J. L. Elechiguerra, A. Camacho, K. Holt, J. B. Kouri, J. T. Ramirez and M. J. Yacaman, *Nanotechnology*, 2005, **16**, 2346–2353.

34 B. Bolto, T. Tran, M. Hoang and Z. L. Xie, *Prog. Polym. Sci.*, 2009, **34**, 969–981.

35 A. G. Destaye, C.-K. Lin and C.-K. Lee, *ACS Appl. Mater. Interfaces*, 2013, **5**, 4745–4752.

36 A. Watanabe, S. Morita and Y. Ozaki, *Biomacromolecules*, 2007, **8**, 2969–2975.